Article

Design and analysis of blue InGaN/GaN plasmonic LED for high-speed, high-efficiency optical communications

Lorenzo Ferrari, Joseph Smalley, Haoliang Qian, Atsunori Tanaka, Dylan Lu, Shadi A. Dayeh, Yeshaiahu Fainman, and Zhaowei Liu

ACS Photonics, **Just Accepted Manuscript** • DOI: 10.1021/acsphotonics.8b00321 • Publication Date (Web): 15 Aug 2018

Design and analysis of blue InGaN/GaN plasmonic LED for high-speed, high-efficiency optical communications

Lorenzo Ferrari,[†,⊥] Joseph S. T. Smalley,[‡,¶,⊥] Haoliang Qian,[‡] Atsunori Tanaka,[†] Dylan Lu,[‡,§] Shadi Dayeh,[‡,†] Yeshaiahu Fainman,[‡] and Zhaowei Liu[*,‡,†,∥]

Materials Science and Engineering, University of California, San Diego, 9500 Gilman Drive, La Jolla, CA 92093-0418, USA, Department of Electrical and Computer Engineering, University of California, San Diego, 9500 Gilman Drive, La Jolla, CA 92093-0407, USA, Department of Mechanical Engineering, University of California, Berkeley, 6141 Etcheverry Hall, Berkeley, CA 94720-1740, USA, Department of Chemistry, University of California, Berkeley, 419 Latimer Hall, Berkeley, CA 94720-1460, USA, and Center for Memory and Recording Research, University of California, San Diego, 9500 Gilman Drive, La Jolla, CA 92093-0401, USA

E-mail: zhaowei@ucsd.edu

Abstract

We design, fabricate and analyze a nanostructured plasmonic light emitting diode (LED) that simultaneously increases the modulation speed and radiative efficiency,

[*]To whom correspondence should be addressed
[†]UCSD Materials Science and Engineering
[‡]UCSD Electrical and Computer Engineering
[¶]Present: UCB Mechanical Engineering
[§]Present: UCB Chemistry
[∥]UCSD CMRR
[⊥]These authors equally contributed to the work.

compared to conventional LEDs and unpatterned plasmonic LEDs respectively. Our structure, optimized to ensure its integrability with electrical contacts, couples an InGaN/GaN blue LED with a Ag nanohole grating. Through spatio-temporally resolved photoluminescence measurements, we determine a 40-fold decrease in spontaneous emission lifetime, which sets an upper bound to the direct modulation bandwidth in the GHz regime. Additionally, through careful optimization of the plasmonic nanohole grating, we demonstrate a 10-fold increase in outcoupling efficiency relative to an LED with an unstructured plasmonic film. Our work bridges the plasmonic metamaterial and III-nitride semiconductor communities, laying the groundwork for high-speed, high-efficiency blue plasmonic LEDs for applications in visible light communication and beyond.

Keywords: Plasmonics, photonics, LED, optical communication, visible light communication, high-speed.

The widespread adoption of visible light communication (VLC) systems based on light emitting diode (LED) transmitters requires the simultaneous increase in efficiency and speed of the optical source.[1,2] Efficiency is measured by the external quantum efficiency (EQE) η_{EQE},[3] while speed is quantified by the 3dB modulation bandwidth f_{3dB}.[4] Most research on the indium gallium nitride (InGaN) system, suitable for blue and green emission, has focused on improving the EQE because this metric, and its dependence on the injection current density J_{inj}, is one of the most important factors for the growth of LEDs as an illumination source for general lighting purposes.[3] While the market for lighting exceeds many billions of dollars and general illumination accounts for 20% of U.S. electrical energy consumption,[3] the modulation rate of LEDs is poised to grow in importance due to the need to couple information processing with illumination. An LED with $f_{3dB} \sim$ GHz, incorporated as the light source in an optical transceiver, can enable a plethora of VLC applications: from chip-to-chip wireless communications in data centers to smart automotive lighting, from safe and RF interference-free wireless local area networks in hospitals and offices to underwater optical communications for the exploration, inspection and maintenance of offshore oil

fields.[1,2] Therefore, strategies that advance efficiency and speed simultaneously are much sought after.

Plasmonic and hyperbolic metamaterials (MMs) have gained much attention over the past decade because of their ability to dramatically enhance light-matter interaction.[5] The increased photonic density of states provided by metals, which can be further enhanced and wavelength-tuned with hyperbolic media,[6] enables the controlled reduction of the spontaneous emission lifetime τ_{sp} of a quantum light source (fluorescent molecule, quantum dot, quantum well, nitrogen-vacancy center in diamond[7]), essential for high-speed devices. Lifetime reductions of 10 to 100 times relative to the vacuum have been reported using various realizations of plasmonic and hyperbolic MMs.[8–11] In most cases, however, unpatterned structures demonstrated to increase the emission speed suffer from low radiative efficiency, and the mechanisms leveraged to overcome such limitations, including surface texturing[12] or the use of nanoparticles in lieu of patterned films,[13] hinder their integrability with electronics. On the other hand, metallic nanostructured films known to enhance the emission efficiency of LEDs[14,15] have not been simultaneously optimized to yield an improved speed performance. Therefore, to enable electrically-driven LED sources for fast optical transmitters, a design is needed that enhances modulation speed while preserving at the same time a high radiative efficiency.

The recent demonstration of a light-emitting hyperbolic metasurface, based on nanostructured silver (Ag) and indium gallium arsenide phosphide (InGaAsP) quantum wells,[12] shows that III-V compound semiconductors are a promising candidate for simultaneously efficient and fast LEDs. Moreover, the anisotropic polarization response observed in the metasurface can boost the transmission rate of LEDs used in VLC by introducing an additional degree of freedom (light polarization) for encoding information. However, VLC requires translation of this technology to visible frequencies. Designs that simultaneously yield improved speed and light output at blue wavelengths have been evoked, but they remain the subject of theoretical studies.[16]

In this work we experimentally demonstrate a novel plasmonic LED (PLED) configuration, incorporating a Ag nanohole grating within an InGaN/GaN LED. The PLED exhibits a simultaneous increase in efficiency and speed, compared to conventional LEDs with and without unpatterned plasmonic inclusions, respectively. Through spatio-temporally resolved photoluminescence (PL) measurements, we determine a 40-fold decrease in spontaneous emission lifetime, which sets an upper bound to the modulation bandwidth in the GHz regime. Additionally, through careful optimization of the plasmonic nanohole grating, we demonstrate a 10-fold increase in outcoupling efficiency relative to a flat plasmonic film. The present study bridges the plasmonic metamaterial and III-nitride semiconductor communities, laying the groundwork for high-speed, high-efficiency blue LEDs for VLC applications.

PLASMONIC LED DESIGN

We consider a PLED system formed by an InGaN/GaN LED and a nanostructured Ag plasmonic film. The LED consists of an nGaN layer grown on a sapphire substrate, followed by an InGaN/undoped GaN multiple quantum well (MQW) heterostructure and a pGaN layer, as detailed in the *Materials and methods* section. A PLED design simultaneously capable of high-speed and efficient operation must synthesize a fundamental dichotomy between plasmonic and electronic requirements. On the one hand, the near-field coupling between the MQW emitting region and the pGaN/Ag interface, which supports surface plasmon polaritons (SPPs),[17] is maximized as their distance is minimized. Such distance, coinciding with the pGaN layer thickness t_{pGaN}, should be shorter than the SP penetration depth in GaN, given by[18]

$$t_{plas} = \frac{\lambda_0}{2\pi}\sqrt{\frac{\varepsilon'_{GaN} - \varepsilon'_{Ag}}{\varepsilon'^2_{GaN}}} \approx 37 \text{ nm}, \quad (1)$$

where $\lambda_0 = 450$ nm, and ε'_{GaN}, ε'_{Ag} are the real parts of the permittivity at λ_0 in the pGaN and Ag layers, respectively.[19,20] On the other hand, to maintain proper electronic transport,

the pGaN layer should be thicker than the p-side depletion width of the diode, given by[21]

$$t_{elec} = \sqrt{\frac{2\varepsilon'_{GaN} V_{bi} N_D}{qN_A(N_A + N_D)}} \approx 70 \text{ nm}, \tag{2}$$

where $V_{bi} = 3.3$ V is the built-in voltage, $N_D \approx 6 \times 10^{18}$ cm^{-3} and $N_A \approx 5 \times 10^{17}$ cm^{-3} are the carrier concentrations in the nGaN and the pGaN, respectively (see *Materials and methods* section), and $q = 1.6 \times 10^{-19}$ C is the fundamental charge. The built-in voltage is given by $V_{bi} = (k_B T/q) \ln[(N_A N_D)/n_i^2]$, where $k_B T = 0.026$ eV at room-temperature and $n_i \approx 2.25 \times 10^{-10}$ cm^{-3} is the intrinsic carrier concentration.[22]

To circumvent this inherent conflict, past authors have experimentally explored a design with Ag nanoparticles embedded in undoped GaN,[21] or theoretically envisioned a device based on side-emitting microtubules.[16] We instead propose patterning nanoholes through the pGaN layer to the MQW region, followed by coating the holes with a thin Ag film

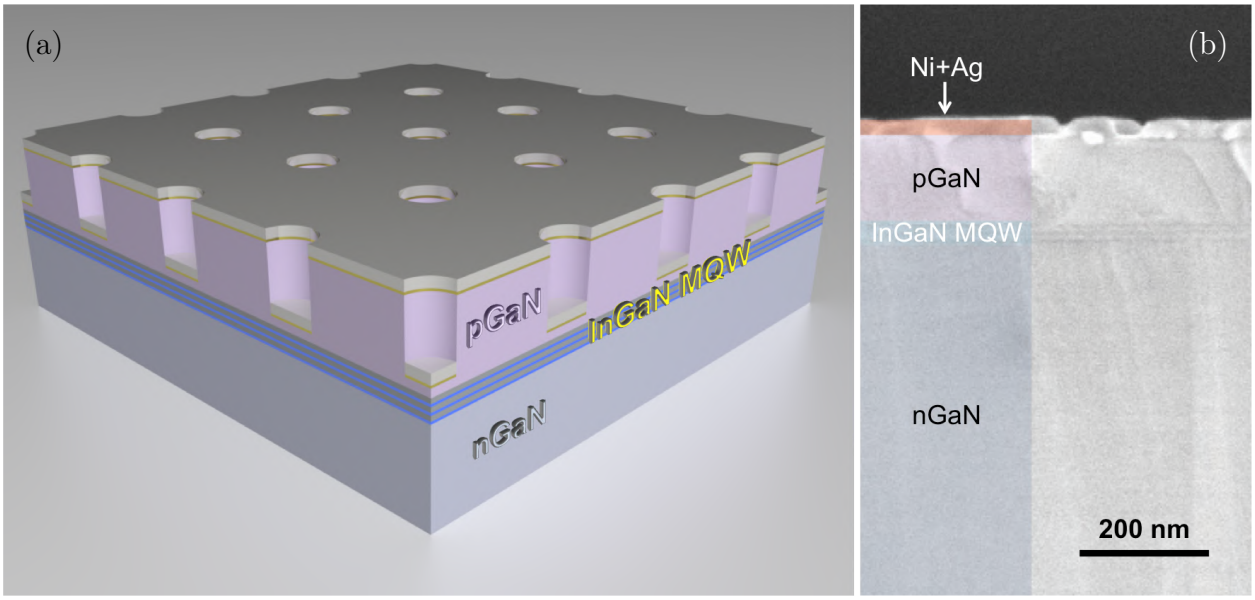

Figure 1: (a) Schematic of the LED with the nanopatterned plasmonic film. Bottom to top: nGaN layer (grey), three InGaN quantum well (blue) - GaN quantum barrier (dark grey) pairs, pGaN (violet). The thin bilayer deposited above the pGaN surface and inside the holes is made of Ni (ochre) and Ag (silver gray). (b) Ultra-high resolution scanning electron microscope (UHR SEM) cross section of the cleaved sample, in a region without gratings. The different components of the structure are highlighted in false color on the left.

(Fig. 1(a)). Our solution leverages the nanostructured nature of the Ag film, necessary to outcouple SPPs into the far field. Our design divides the PLED in two vertical volumes: a "plasmonic" one, occupied by the nanoholes, where the MQW-Ag film distance can be arbitrarily controlled, and an "electronic" one, free from nanoholes, where the diode behavior is preserved. While such general approach conveniently enables a plasmonic-electronic tradeoff, a geometric optimization of the nanoholes is still required, to maximize SPP excitation and outcoupling. Three hole parameters control the interaction between the MQW and the nanopatterned Ag film: hole diameter d_h, hole pitch p_h and hole depth d_{etch}. For the present study we select, aided by numerical optimization, a value for d_h and one for p_h which ease PLED fabrication while still supporting MQW-nanostructure coupling, and we experimentally optimize d_{etch}. We expect a further enhancement of the PLED performance once, based on the results of this work, d_h and p_h are also experimentally optimized.

To understand the role of d_{etch}, we fabricate, atop an InGaN/GaN LED chip with pGaN thickness $t_{pGaN} = 130 - 140$ nm (Fig. 1(b)), six 6 µm x 6 µm gratings (labeled "II" to "VII"), all with identical hole diameter $d_h = 120$ nm and pitch $p_h = 300$ nm. d_{etch} is increased by a constant step from a value smaller (grating II) to a value larger (grating VII) than t_{pGaN}, in the approximate range $100 - 200$ nm. After nanohole milling, accomplished via focused ion beam (FIB), a 2 nm Ni adhesion layer followed by a 20 nm Ag layer is deposited everywhere on the sample (*Materials and methods* section). In the following we show through experimental characterization and numerical verification that the outcoupling exhibits a non-monotonic dependence on hole depth, and we determine the value of d_{etch} that maximizes the excitation and far-field scattering of SPPs. This optimized efficiency, in addition to the high-speed capability and sufficient pGaN thickness for diode behavior, makes our PLED design viable for practical VLC applications.

RESULTS AND DISCUSSION

Static and spatio-temporally resolved photoluminescence. The static PL spectrum of the PLED is collected with the standard micro-PL setup detailed in the *Materials and*

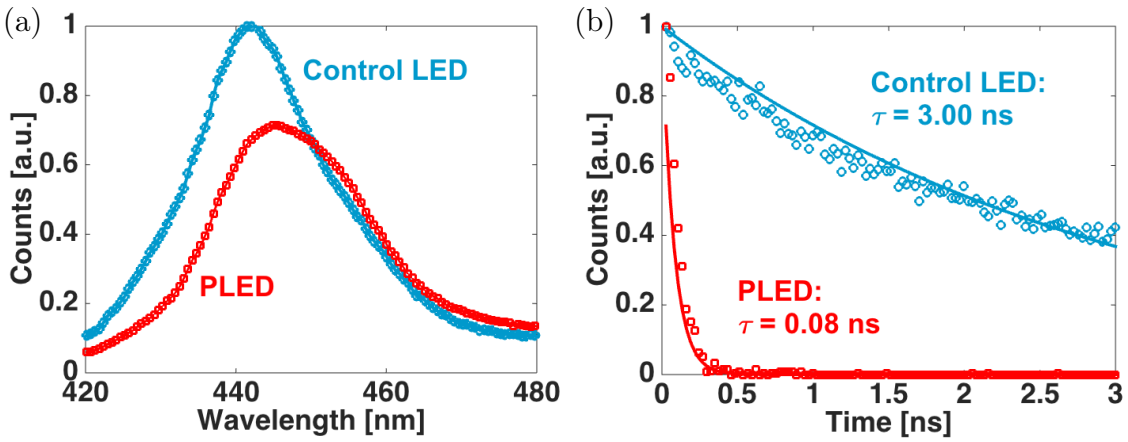

Figure 2: Comparison between control LED and PLED. (a) Photoluminescence intensity spectra and (b) time resolved photoluminescence at the vacuum wavelength $\lambda_0 = 450$ nm. In (b), the circles and squares represent experimental data points, while the solid curves are mono-exponential fits to the data.

methods section. Fig. 2(a) compares the PL emission from a control LED, consisting of the identical III-nitride heterostructure with neither nanostructuring nor metal, with the one from a non-structured area of the PLED, where only a flat Ag film is present. The PLED gratings cannot be individually probed with our micro-PL setup, as the size of the excitation beam is much larger than their area. With respect to the control LED, the PLED emission exhibits a slight red-shift and a decrease in intensity. The red-shift may be attributed to small local variations in the LED structure and composition, resulting in an emission wavelength gradient of few nm, as well as to local heating and to energy mismatch between the MQW emission and the surface plasmon resonance. The intensity decrease may be traced to quenching effects, induced on the GaN surface by the Ni hard mask strip off via Ni etchant (*Materials and methods* section). We observe that, for the patterned areas, another source of quenching is the surface damage caused by FIB milling. The kinetic energy transfer from the Ga^+ ions to the LED crystal lattice generates a thin (few nm) damaged amorphous layer on the etched surface, which can be removed by post-FIB wet etching in a heated KOH solution.[23–25]

Because the PL peak of the PLED occurs at $\lambda_0 = 450$ nm, this is the chosen detection

wavelength for the following spatio-temporally resolved PL characterization. By means of the setup described in the *Materials and methods* section, we perform a raster scan of the PLED area occupied by the gratings, detecting at each step the PL lifetime and intensity. The lifetime values measured in the grating regions are comparable for all gratings, regardless of their hole depth. This indicates that, at $\lambda_0 = 450$ nm, the convolution of the different Purcell factor contributions, resulting from the interaction between the emitters space distribution and the metallic inclusions, yields a net Purcell factor that stays approximately constant across the hole depths. The hole pitch, identical for all gratings, plays indeed a dominant role in controlling the lifetime reduction,[8] while the depth mainly impacts the efficient outcoupling of SPPs into the far field, as we demonstrate later. A representative decay curve of the PLED, measured on grating II, is compared in Fig. 2(b) with that of the control LED: the respective lifetimes are $\tau_{PLED} = 0.08$ ns and $\tau_{cont} = 3$ ns, corresponding to an almost 40-fold shortening.

The relation of measured PL lifetime to modulation bandwidth is a complicated function that depends on the optical, electrical, and thermal properties of the LED, which are influenced by device geometry and packaging. However, the maximum modulation bandwidth may be easily found through a rate equation model derived for cavity-based LEDs.[26] The frequency response H is given by

$$H(\omega) = \frac{\Gamma}{\tau_c} = \frac{1}{\left(1 + \frac{i\omega}{\gamma_c}\right)\left(1 + \frac{i\omega}{\gamma_{sp}}\right)}, \tag{3}$$

where ω is the angular frequency ($\omega = 2\pi f$) and Γ is the modal confinement factor. The cavity and spontaneous emission decay rates, γ_c and γ_{sp}, are respectively $\gamma_c = \tau_c^{-1}$ and

$$\gamma_{sp} = \tau_{sp}^{-1} = \gamma_{rad} + \gamma_{n-rad}, \tag{4}$$

where τ_c is the lifetime of photons in the cavity, τ_{sp} is the spontaneous emission lifetime, and γ_{rad} and γ_{n-rad} are the rates at which electron-hole pairs entering the active region recombine

radiatively and non-radiatively. In the absence of a cavity, the quality factor $Q = \omega/\gamma_c$, is determined by the natural linewidth of emission, which corresponds to the full-width at half-maximum (FWHM) of the PL spectra of Fig. 2(a). From Fig. 2(a), $\tau_c \approx [c/(430\text{ nm} - c/(455\text{ nm})] = 3.9 \times 10^{-15}$ s, which is much smaller than τ_{sp}, of the order of tens of ps. Hence the frequency response is limited by γ_{sp}. Then, in this limit, we can write the maximum 3dB modulation bandwidth f'_{3dB} as

$$f'_{3dB} = max[f_{3dB}] = \frac{\sqrt{3}}{2\pi\tau_{eff}}. \quad (5)$$

where $\tau_{eff} = \tau_{sp}/2.5$ is the differential carrier lifetime.[27,28] The experimentally measured lifetimes imply that the PLED can achieve a 3dB bandwidth of about 8.5 GHz. We note that the modal confinement factors of the control LED and the PLED are essentially identical, so that the Γ term has a negligible effect on the comparison.

The high-speed potential of the PLED can be fully harnessed only if effective light outcoupling is provided. In order to identify the best extraction geometry, we study the impact of the hole depth on PL intensity. Fig. 3 presents the spatial mapping of PL across the six nanohole gratings. As can be inferred from the color contrast, all the nanostructures provide an enhanced outcoupling compared with the neighboring unpatterned areas. However, the monotonic increase in d_{etch} from the first (grating II) to the last (grating VII) grating results in a non-monotonic PL trend. The intensity is comparable for gratings II, III, and IV, reaches a maximum at grating V, then becomes smaller for gratings VI and VII. The maximum signal detected at grating V is about 10 times the signal detected away from the gratings on the flat Ag film.

Structural analysis of the plasmonic LED. To understand the origin of this behavior, and explain how the MQW-nanostructure interaction is controlled by the hole depth, we conduct a cross-sectional analysis of the best performing grating (grating V), and of the two gratings with depths immediately smaller and larger (grating IV and VI, respectively).

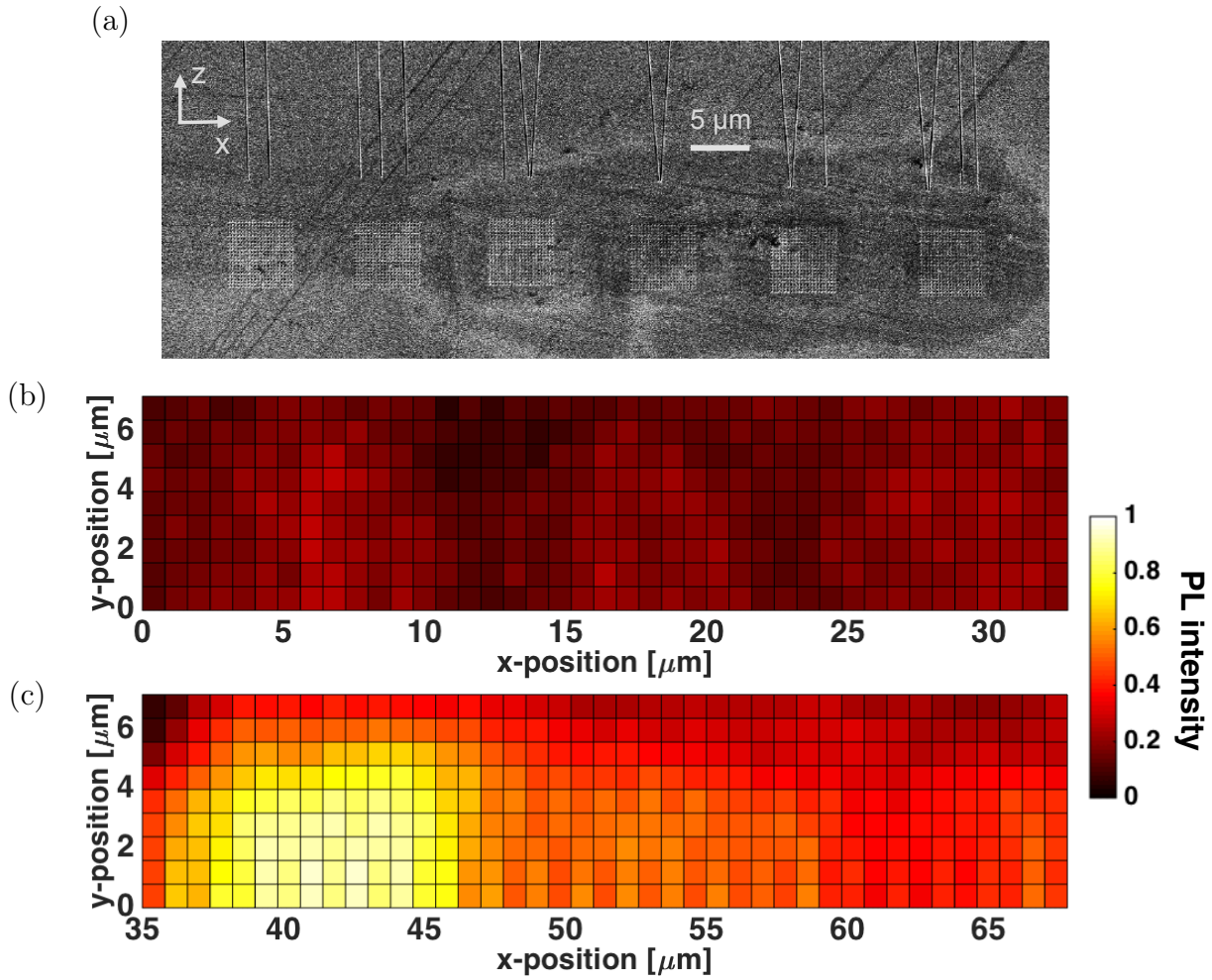

Figure 3: PL intensity mapping at $\lambda_0 = 450$ nm of different PLED geometries. (a) SEM image of the six nanohole gratings, milled with increasing hole depth from left to right. (b) Spatially resolved PL intensity of gratings II through IV, and (c) of gratings V through VII. PL intensity is plotted on a logarithmic scale and is normalized to the minimum, which occurs between gratings II and III.

The details of two cross-sectioned nanoholes of gratings IV, V and VI, highlighted by a blue frame in Figs. 4(a), (b) and (c), are presented in Figs. 4(d), (e) and (f) respectively. By effect of photoablation, not only on the top surface, but also at the bottom of the nanoholes has Ag either sublimated of melted and reaggregated in small inclusions, as the brightest features in Figs. 4(d) and 4(e) indicate. For each of the three gratings, we image at 240,000x magnification the cross-sectioned nanoholes, and measure the separation between their bottom and the pGaN surface. Within the limits imposed by image resolution and

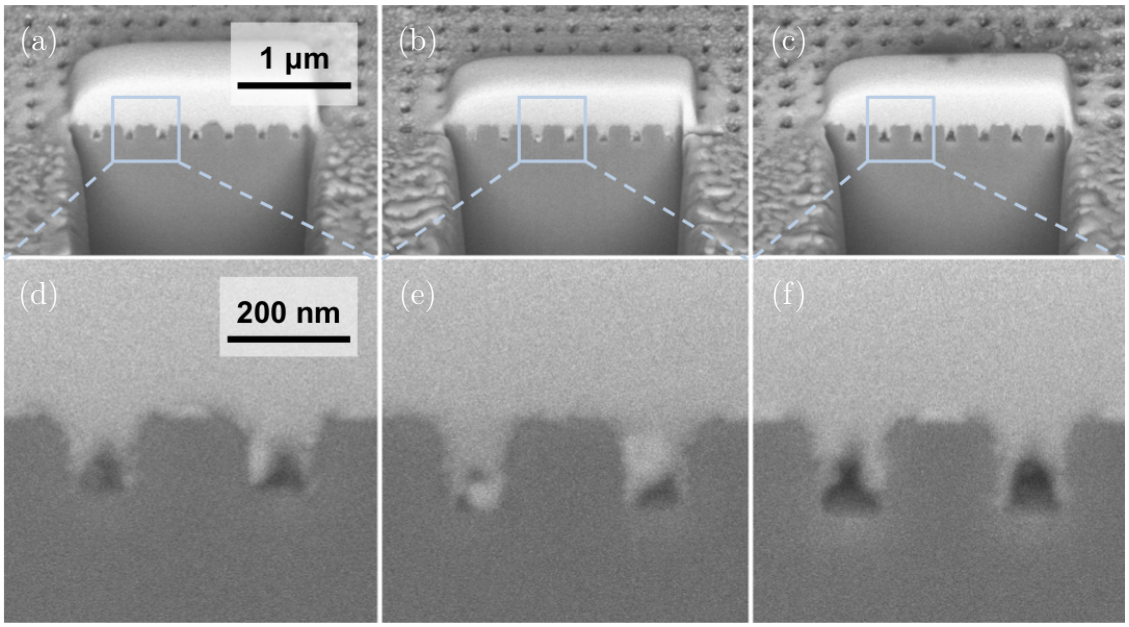

Figure 4: (a) Back-scattered electrons (BSE) SEM image (52° tilt) of a portion of grating IV, (b) V and (c) VI, cross-sectioned via FIB to measure the hole depth. The cut area and its surroundings show the damage caused to the grating region by the PL mapping. A Pt film (bright volume on the grating) was deposited via electron-assisted chemical vapor deposition (CVD) prior to the cut, to protect the grating surface and ensure optical contrast for the hole cross-section. (d) BSE SEM detail (52° tilt) of the hole cross-section of grating IV, (e) grating V and (f) grating VI. Due to the aspect ratio larger than 1:1, the Pt coating only partially fills the holes, leaving voids at the bottom.

contrast, we determine the hole depths of gratings IV, V and VI to be in the range 145-155 nm, 165-175 nm and 180-185 nm, respectively. It is impossible to discern in the BSE SEM pictures the pGaN, MQW and nGaN regions; however, we know that the pGaN thickness is $t_{pGaN} = 130 - 140$ nm, and the MQW thickness is 36 nm (*Materials and methods* section). Recalling that the Ag film thickness is 20 nm, we conclude that the PL intensity is maximized when so is the overlap between the Ag nanodisk inclusions at the bottom of the holes and the MQW volume.

To gain further insight in our result, we study the MQW-nanostructured plasmonic film coupling by means of 3D finite element simulations (Comsol Multiphysics). The periodicity of the grating is modeled with periodic boundary conditions. The unit cell of the grating, with side $p_h = 300$ nm, contains a GaN block, patterned with a nanohole with fixed diameter

$d_h = 120$ nm and variable depth d_{etch}. The GaN surface and the bottom of the hole are coated with a 20 nm Ag film; the permittivities of GaN and Ag are taken from [19] and,[20] respectively. The MQW emission is modeled with an electric dipole, fixed at a vertical distance $d_{es} = 140$ nm from the GaN surface, and at a horizontal distance $d_{eh} = 10$ nm from the hole. To reproduce our experimental study, we progressively vary d_{etch} from a smaller value than d_{es} to a larger one, leaving all other geometrical parameters unaltered, and collect the power emitted by the dipole-nanostructure system through the bottom of the simulation domain. In analogy with the PL intensity plots of Fig. 3, we define radiative enhancement (RE) as the collected power normalized to the power detected in the absence of nanostructures, namely for a dipole embedded in a bulk GaN block with a flat Ag film on top. In Fig. 5(a), the radiative enhancement is plotted as a function of the hole etching depth d_{etch}. Each data point is obtained from an equally weighted average over the three Cartesian dipole orientations. The trend resembles our experimental findings: the largest RE is observed at the depths $d_{etch} = 150$, 155 and 160 nm, which maximize the horizontal overlap between the dipole and the Ag nanodisk inclusion. We notice that the magnitude of the enhancement is smaller than the one experimentally detected. This quantitative discrepancy originates from our modeling of the PLED, based on material (permittivity values taken from literature rather than experimentally determined), structural (replacement of the exciton distribution within the entire MQW volume with an individual 1D dipole, and of the LED layers with a homogeneous GaN volume, neglecting the effects of stress and strain and the perturbation of crystalline order induced by ion milling; simulation focused on the dipole emission, neglecting any excitation efficiency considerations) and operational (power detection angle limited by the use of a unit cell) approximations. Nonetheless, the qualitative picture confirms and strengthens the interpretation of our results. Fig. 5(b) compares the power distribution of the simulated dipole-nanostructure system at three different etching depths and for the three Cartesian dipole orientations. At $d_{etch} = 120$ nm and $d_{etch} = 180$ nm, when the etching depth is respectively shorter and larger than d_{es}, the emitter-Ag nanodisk coupling is limited. At

d_{etch} = 160 nm instead, when the nanodisk is next to the dipole, the gain-mode overlap is maximized, resulting in increased emission.

Discussion. By separating the device volume in "plasmonic" and "electronic" domains, our PLED design enables a simultaneous increase in modulation speed and output intensity, while still preserving an effective diode structure. Spontaneous emission lifetime, which sets the optical limit for the direct modulation bandwidth, can be tuned via the hole grating geometry. A shorter lifetime can be achieved with a shorter grating pitch;[8] the diameter does not play a significant role for shallow holes, while for deep ones a larger radius implies a

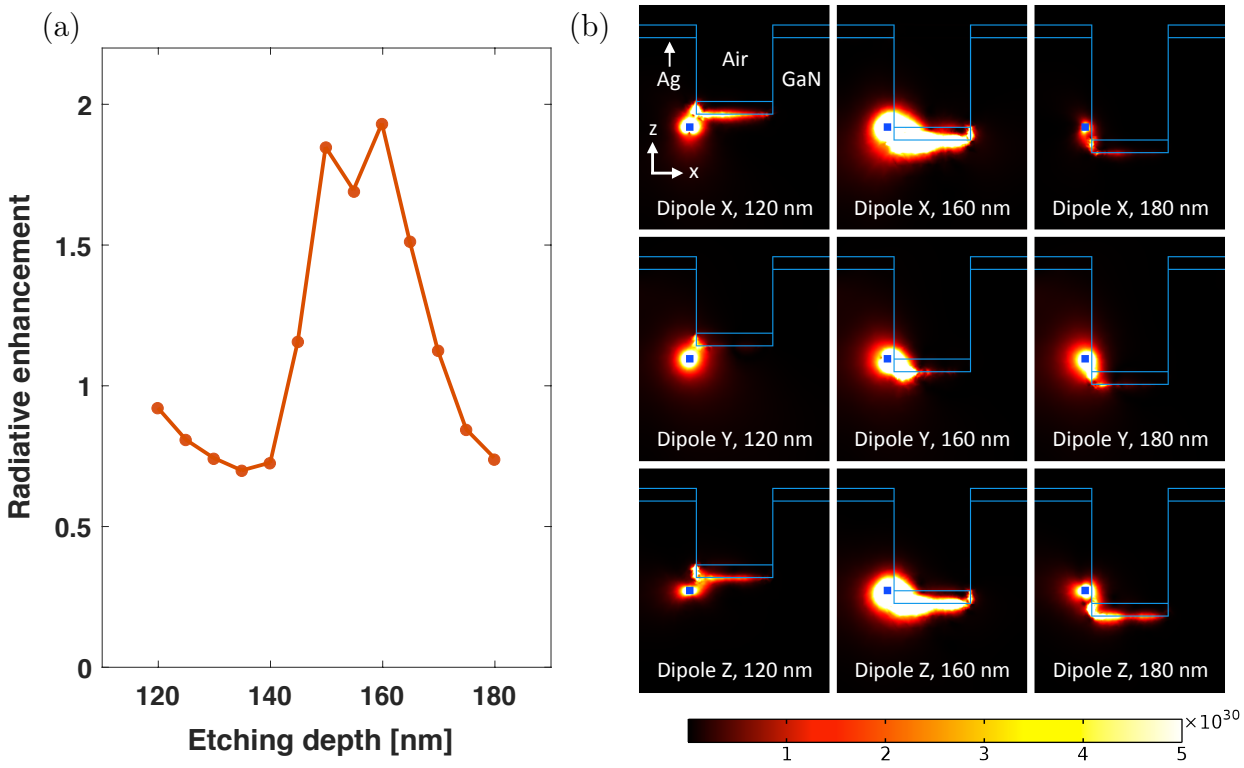

Figure 5: Simulated interaction between a quantum emitter (point dipole) and a Ag plasmonic grating in GaN. The hole diameter and pitch (d_h = 120 nm, p_h = 300 nm), the plasmonic film thickness (t_{Ag} = 20 nm) and the emitter position (emitter-GaN surface vertical distance d_{es} = 140 nm, emitter-hole horizontal distance d_{eh} = 10 nm) are fixed, while the etching depth d_{etch} of the holes is varied across a range of values smaller, equal to and larger than d_{es}. (a) Radiative enhancement as a function of the etching depth of the holes. The values are representative of an isotropic dipole (average over the three Cartesian dipole orientations). (b) Magnitude of the Poynting vector in the xz cross-sectional plane bisecting the unit cell of the grating, for the three Cartesian dipole orientations at selected hole depths (d_{etch} = 120, 160, 180 nm). The dipole position is indicated by a blue square.

reduced lifetime.[29] Interdependence exists, however, between the grating geometry and the pGaN layer thickness. As pointed out earlier, t_{pGaN} needs to be at least larger than the depletion width of the LED, in order to grant a satisfactory carrier injection into the MQW. On the other hand, an arbitrary increase in t_{pGaN} faces nanofabrication limitations. We demonstrated that, to maximize light extraction, the bottom of the nanoholes should reach below the vertical location of the MQW, such that the overlap between the plasmonic film and the emitting volume reaches a maximum. By constraining the hole depth, t_{pGaN} imposes a practical limit also on the hole diameter and pitch. Depth:diameter aspect ratios larger than 1.5:1 make it progressively harder to ensure the structural integrity of the grating (i.e. to define straight hole walls and sharp edges, which becomes critical as the pitch is decreased since nearest neighbor holes can collapse into each other) and the filling of the nanoholes with plasmonic inclusions. Therefore, the balance between modulation bandwidth, internal quantum efficiency and injection efficiency of the PLED can be controlled with the above-discussed parameters, keeping in mind their strong interplay.

In order to enable direct current modulation, electrical contacts with a ground-signal-ground (GSG) topology, supporting high-speed operation through the minimization of capacitive effects, need to be integrated in the PLED. Our choice of a transparent sapphire substrate (*Materials and methods* section) allows light emission from the bottom of the PLED chip: therefore, a Au pGaN contact can be deposited on top of the plasmonic grating, and further increase radiation extraction by acting as a mirror. Alternatively, a transparent indium tin oxide (ITO) contact can be adopted if top emission is preferred. If a contact is deposited directly on the plasmonic grating, the filled holes volume becomes a preferential path for current, due to its larger conductivity compared to pGaN. The poor injection efficiency of the "electronic" regions and the shorting of the "plasmonic" ones hamper the functioning of the PLED. A remedy consists in coating a thin (few nm) oxide insulation layer inside the nanoholes prior to the plasmonic film deposition. In this way, the Ag inclusions still overlap horizontally with the MQW volume, but the current flow is confined to the "electronic"

regions with a proper diode structure. To obtain a conformal protection of the bottom and the internal walls of the nanoholes, a SiO_2 or Al_2O_3 layer can be grown by atomic layer deposition (ALD). This step however needs to be followed by directional dry etching of the surface of the PLED, to remove the oxide coating from the top of the "electronic" regions which otherwise cannot be effectively contacted.

An alternative approach to the integration of plasmonic nanostructures in InGaN/GaN LEDs, experimentally explored in,[21] consists in inserting Ag nanoparticles into the LED structure. The inconvenience of this method is that it requires breaking the vacuum in the growth chamber to e-beam evaporate the metallic particles, which can result in the incorporation of impurities within the heterostructure. In addition, the roughness induced by the particles propagates to the upper layers grown on top of them, with obvious consequences for the lattice cristallinity both in the MQW and in the pGaN. Our design instead preserves the planarity of the LED structure, and utilizes a plasmonic grating whose geometry can be accurately and reproducibly controlled. In view of mass producing the PLED, low throughput techniques such as FIB (which can also cause ion implantation in the LED crystal lattice) or e-beam lithography are not a convenient choice to inscribe a nanohole grating. Large-scale, large-area alternatives, such as nanoimprint lithography (NIL) or direct laser writing lithography[30] can enable high throughput fabrication.

The PLED design detailed in this work enables the implementation of blue LED transmitters in VLC systems. To increase the number of wavelength channels, it is either possible to engineer the InGaN emission (limitedly to the UV-blue-green spectral region) or to resort to a different semiconductor platform (for the red-infrared region). However, owing to its fixed plasmonic properties, Ag effectively enhances the modulation bandwidth only at blue frequencies. Substitution of the Ag thin film with a multilayer hyperbolic MM allows tuning the wavelength of maximum lifetime reduction across the rest of the light spectrum. For example, a Ag/Si multilayer red-shifts the plasmonic resonance monotonically with the amount of Si, allowing peak bandwidth enhancements at green and red frequencies.[8,31]

The density of information of a monochromatic PLED channel can be increased by encoding in the emitted light two different polarizations. To this end, the nanohole grating can be replaced with chiral plasmonic metasurfaces, patterned with spiral features that induce a right-handed or a left-handed circular polarization.[32–34] Compared with linear polarization, circular polarization exhibits a higher degree of persistence in scattering environments,[35] and is therefore more suited for VLC. Not only spin angular momentum (right- or left-handedness) can be encoded with plasmonic metasurfaces, but also and most importantly orbital angular momentum (OAM), related to the helicoidal shaping of the emitted wavefront.[36] OAM is associated with a quantum number which can assume any integer value from 0 to infinity, providing for a given light frequency a number of information channels that is, in principle, unlimited.

CONCLUSIONS

In conclusion, the present work introduced a novel plasmonic LED design that combines a blue InGaN/GaN LED with a nanostructured film, consisting of a nanohole grating coated with a thin Ag layer. By decoupling the device volume into "plasmonic" and "electronic" regions, the PLED is simultaneously capable of increased modulation speed, compared to a conventional LED, and increased light output, compared to a plasmonic LED with a flat Ag film, while preserving an effective p-i-n junction structure. In order to optimize light extraction, we fabricated six plasmonic gratings with identical pitch and hole diameter, and variable hole depth. Time-resolved photoluminescence measurements at the peak emission wavelength $\lambda_0 = 450$ nm predicted an almost 40-fold enhancement in the limit 3dB modulation bandwidth for all the gratings. A spatial mapping of the PL intensity at $\lambda_0 = 450$ nm, combined with a cross-sectional analysis of the fabricated structures, revealed that light extraction is maximized when the Ag nanodisk inclusions inside the holes overlap with the MQW volume, rather than sitting above or below it. This finding is corroborated by 3D numerical simulations, showing an identical trend for a dipole-plasmonic nanohole system. We discussed the mutual influence between the pGaN thickness and the grating geometrical

parameters, and how the introduction of an insulation layer inside the nanoholes is required to enable effective electrooptical performance. Our study paves the way for a practical implementation of plasmonically-enhanced high-speed, high-efficiency incoherent sources in VLC systems. Future work will include the design, optimization and testing of electrical contacts suitable for high-speed modulation. We will also extend the PLED design to green and red wavelengths by replacing the Ag film with a properly chosen multilayer hyperbolic MM.

FUNDING SOURCES

The authors acknowledge financial support from the NSF Award DMR-1610538.

MATERIALS AND METHODS

LED growth. The GaN LED was grown on a double side polished (DSP) c-sapphire wafer, of diameter 2 in and thickness 300 µm, with a 3 x 2-in Thomas Swan/Axitron close-coupled showerhead (CCS) metal-organic chemical vapor deposition (MOCVD) system. The LED structure, from the substrate upwards, consists of a 1 µm undoped GaN buffer layer and a 600 nm Si-doped nGaN layer ($N_D \approx 6 \times 10^{18}$ cm^{-3}), followed by 3 InGaN/undoped GaN (2 nm/10 nm) quantum well/quantum barrier (QB) layers.[37] The MQW active region is capped with a Mg-doped pGaN layer ($N_A \approx 5 \times 10^{17}$ cm^{-3}), whose thickness varies across the wafer between 130 and 140 nm. The growth temperature of the InGaN layer was adjusted to 730°C to tune the emission wavelength to about 450 nm. The wafer was annealed inside the MOCVD chamber at 750°C under N_2 flow to activate the Mg dopants in the pGaN layer.

Patterning of plasmonic grating. The growth wafer was diced into 1x1 cm^2 samples and subsequently coated with a 10nm Ni sacrificial mask by e-beam evaporation (Temescal BJD 1800, rate = 2 Å / s), to protect the LED surface. Six 6 µm x 6 µm gratings were patterned on the LED with a focused ion beam system (FEI Scios DualBeam FIB/SEM). Each grating consists of a 20 x 20 array of holes, with pitch 300 nm and hole diameter 120 nm, etched with a Ga ion beam at a voltage of 30 kV and a current of 1.5 pA. What differentiates the

gratings is the hole etching depth, varied from values smaller to larger than the pGaN layer thickness. Once the patterning was complete, the Ni mask was wet etched in Ni etchant, and a Ni adhesion layer (2 nm, rate = 0.2 Å / s) followed by a Ag plasmonic film (20 nm, rate = 0.5 Å / s) was deposited on the gratings by e-beam evaporation.

Static photoluminescence. The PL spectra of Fig. 2(a) were measured with a micro-PL system. The excitation light, generated by a mercury lamp (X-cite 120 Q), was filtered at 405 nm (405/10 nm bandpass filter, Semrock Brightline) and focused on the sample. The emitted light was collected with a 50x, 0.55 NA objective (Zeiss Epiplan Neofluar) and spectrally analyzed by a Czerny-Turner spectrograph (Andor Shamrock 303i): after entering a 20 µm aperture, radiation was spatially separated by a blazed diffraction grating (150 lines/mm, blaze wavelength $\lambda_b = 500$ nm), and detected with a charge-coupled device (CCD) camera (Andor Newton). A dichroic beam splitter (405 nm, Semrock Brightline) and a long-pass filter (409 nm, Semrock Brightline) ensured that the portion of the excitation light reflected off the sample was removed from the analyzed signal.

Spatio-temporally resolved photoluminescence. Spatially- and temporally-resolved PL was measured by first illuminating the sample with a femtosecond Ti:sapphire laser (Spectra Physics Mai Tai) of 800 nm wavelength, 80 MHz repetition rate, and 100 fs pulse width. Due to two-photon absorption, the sample fluoresced at wavelengths between 400 and 500 nm. Fluorescence at the emission wavelength of 450 nm was collected through the bottom of the sample with a 20x, 0.45 NA objective, then sent to a monochromator (Horiba) and finally detected with an electrically cooled photo-multiplier tube (PMT). The Ti:sapphire laser was synched (TB-01 Pulse Converter Module) with a time-correlated single-photon detector (Horiba High Throughput TCSPC controller) providing 27 ps timing resolution. The beam position relative to the sample was controlled by moving the sample stage with a two-axis piezo-electric motor (Mad City Labs NanoDrive) with an 800 nm step size. Alignment of the pump beam and sample was achieved with a microscope (Olympus 1X81) and a complementary metal-oxide-semiconductor (CMOS) camera (μEye).

Cross-sectional analysis. After completing the PL characterization, and repeating it to confirm its result, we deposited a thick (several hundreds of nm) Pt layer on a portion of the grating via the electron-assisted CVD capability of our FIB tool. The function of this coating is twofold: to protect the grating surface during the cut, and to ensure optical contrast with the InGaN/GaN heterostructure by filling the nanoholes. We then defined by means of FIB a vertical cross section along the hole diameter. We observe that, despite a preliminary optimization of the electron deposition current, the larger than 1:1 aspect ratio of the nanoholes forbids Pt from filling them completely. This however does not prevent the identification of their bottom with sufficient accuracy for depth measuring purposes. We also notice that the repeated raster-scanning of the grating area with the two-photon excitation beam caused a progressive damage to the Ag film, manifest both outside of the patterned region, where the Ag film results thinned, and inside such region, where the film has almost completely disappeared.

References

(1) Khan, L. U. Visible light communication: applications, architecture, standardization and research challenges. *Digital Communications and Networks* **2017**, *3*, 78 – 88.

(2) Pathak, P. H.; Feng, X.; Hu, P.; Mohapatra, P. Visible Light Communication, Networking, and Sensing: a Survey, Potential and Challenges. *IEEE Communications Surveys Tutorials* **2015**, *17*, 2047–2077.

(3) Pimputkar, S.; Speck, J. S.; DenBaars, S. P.; Nakamura, S. Prospects for LED lighting. *Nat. Photon.* **2009**, *3*, 180–182.

(4) Gong, C.-S. A.; Lee, Y.-C.; Lai, J.-L.; Yu, C.-H.; Huang, L. R.; Yang, C.-Y. The High-efficiency LED Driver for Visible Light Communication Applications. *Scientific Reports* **2016**, *6*, 30991.

(5) Ferrari, L.; Wu, C.; Lepage, D.; Zhang, X.; Liu, Z. Hyperbolic metamaterials and their applications. *Progress in Quantum Electronics* **2015**, *40*, 1–40.

(6) Krishnamoorthy, H. N. S.; Jacob, Z.; Narimanov, E.; Kretzschmar, I.; Menon, V. M. Topological Transitions in Metamaterials. *Science* **2012**, *336*, 205–209.

(7) Shalaginov, M. Y.; Ishii, S.; Liu, J.; Liu, J.; Irudayaraj, J.; Lagutchev, A.; Kildishev, A. V.; Shalaev, V. M. Broadband enhancement of spontaneous emission from nitrogen-vacancy centers in nanodiamonds by hyperbolic metamaterials. *Applied Physics Letters* **2013**, *102*, 173114.

(8) Lu, D.; Kan, J. J.; Fullerton, E. E.; Liu, Z. Enhancing spontaneous emission rates of molecules using nanopatterned multilayer hyperbolic metamaterials. *Nat. Nano.* **2014**, *9*, 48–53.

(9) Sreekanth, K. V.; Krishna, K. H.; De Luca, A.; Strangi, G. Large spontaneous emission rate enhancement in grating coupled hyperbolic metamaterials. *Scientific Reports* **2014**, *4*, 6340.

(10) Galfsky, T.; Krishnamoorthy, H. N. S.; Newman, W.; Narimanov, E. E.; Jacob, Z.; Menon, V. M. Active hyperbolic metamaterials: enhanced spontaneous emission and light extraction. *Optica* **2015**, *2*, 62–65.

(11) Galfsky, T.; Sun, Z.; Considine, C. R.; Chou, C.-T.; Ko, W.-C.; Lee, Y.-H.; Narimanov, E. E.; Menon, V. M. Broadband Enhancement of Spontaneous Emission in Two-Dimensional Semiconductors Using Photonic Hypercrystals. *Nano Letters* **2016**, *16*, 4940–4945.

(12) Smalley, J. S. T.; Vallini, F.; Montoya, S. A.; Ferrari, L.; Shahin, S.; Riley, C. T.; Kanté, B.; Fullerton, E. E.; Liu, Z.; Fainman, Y. Luminescent hyperbolic metasurfaces. *Nat. Commun.* **2017**, *8*, 13793.

(13) Akselrod, G. M.; Argyropoulos, C.; Hoang, T. B.; Ciracì, C.; Fang, C.; Huang, J.; Smith, D. R.; Mikkelsen, M. H. Probing the mechanisms of large Purcell enhancement in plasmonic nanoantennas. *Nat. Photon.* **2014**, *8*, 835–840.

(14) Cheng-Hsueh, L.; Chia-Chun, L.; Yen-Lin, L.; Yun-Li, L.; Chuan-Pu, L. Enhancement of Green Emission from InGaN/GaN Multiple Quantum Wells via Coupling to Surface Plasmons in a Two-Dimensional Silver Array. *Advanced Functional Materials* **2011**, *21*, 4719–4723.

(15) Chen, H.-S.; Chen, C.-F.; Kuo, Y.; Chou, W.-H.; Shen, C.-H.; Jung, Y.-L.; Kiang, Y.-W.; Yang, C. C. Surface plasmon coupled light-emitting diode with metal protrusions into p-GaN. *Applied Physics Letters* **2013**, *102*, 041108.

(16) Liu, L.; Zhao, L.; Zhu, S.; Yu, Z.; An, P.; Yang, C.; Wu, C.; Li, J. Design of GaN-based surface plasmon LEDs to enhance the modulation bandwidth and light output. *Physica Status Solidi (c)* **2016**, *13*, 283–288.

(17) Zhu, S.-C.; Yu, Z.-G.; Zhao, L.-X.; Wang, J.; Li, J.-M. Enhancement of the modulation bandwidth for GaN-based light-emitting diode by surface plasmons. *Opt. Express* **2015**, *23*, 13752–13760.

(18) Okamoto, K.; Niki, I.; Shvartser, A.; Narukawa, Y.; Mukai, T.; Scherer, A. Surface-plasmon-enhanced light emitters based on InGaN quantum wells. *Nat. Mater.* **2004**, *3*, 601–605.

(19) Djurišić, A.; Chan, Y.; Li, E. Novel model for the optical function of GaN. *Applied Physics A* **2002**, *74*, 669–674.

(20) Johnson, P. B.; Christy, R. W. Optical Constants of the Noble Metals. *Phys. Rev. B* **1972**, *6*, 4370–4379.

(21) Kwon, M.-K.; Kim, J.-Y.; Kim, B.-H.; Park, I.-K.; Cho, C.-Y.; Byeon, C. C.; Park, S.-J. Surface-Plasmon-Enhanced Light-Emitting Diodes. *Advanced Materials* **2008**, *20*, 1253–1257.

(22) Hou, H. W.; Liu, Z.; Teng, J. H.; Palacios, T.; Chua, S. J. High Temperature Terahertz Detectors Realized by a GaN High Electron Mobility Transistor. *Scientific Reports* **2017**, *7*, 46664.

(23) Wang, X. H.; Ning, J. Q.; Xu, S. J.; Choi, H. W. Raman and photoluminescence characterization of focused ion beam patterned InGaN/GaN multi-quantum-wells nanopillar array. *Journal of Applied Physics* **2011**, *110*, 093111.

(24) Kong, D.-J.; Bae, S.-Y.; Kang, C.-M.; Lee, D.-S. InGaN/GaN microcolumn light-emitting diode arrays with sidewall metal contact. *Opt. Express* **2013**, *21*, 22320–22326.

(25) Han, D.; Ma, S.; Jia, Z.; Liu, P.; Jia, W.; Shang, L.; Zhai, G.; Xu, B. Morphologies and optical and electrical properties of InGaN/GaN micro-square array light-emitting diode chips. *Appl. Opt.* **2018**, *57*, 2835–2840.

(26) Lau, E. K.; Lakhani, A.; Tucker, R. S.; Wu, M. C. Enhanced modulation bandwidth of nanocavity light emitting devices. *Opt. Express* **2009**, *17*, 7790–7799.

(27) Agrawal, G. P. *Fiber-Optic Communication Systems*, 4th ed.; Wiley, 2010.

(28) Coldren, L. A.; Corzine, S. W.; Mashanovitch, M. L. *Diode Lasers and Photonic Integrated Circuits*, 2nd ed.; Wiley, 2012.

(29) Lei, D. Y.; Li, J.; Fernández-Domínguez, A. I.; Ong, H. C.; Maier, S. A. Geometry Dependence of Surface Plasmon Polariton Lifetimes in Nanohole Arrays. *ACS Nano* **2010**, *4*, 432–438.

(30) Bagheri, S.; Weber, K.; Gissibl, T.; Weiss, T.; Neubrech, F.; Giessen, H. Fabrication of Square-Centimeter Plasmonic Nanoantenna Arrays by Femtosecond Direct Laser

Writing Lithography: effects of Collective Excitations on SEIRA Enhancement. *ACS Photonics* **2015**, *2*, 779–786.

(31) Ferrari, L.; Lu, D.; Lepage, D.; Liu, Z. Enhanced spontaneous emission inside hyperbolic metamaterials. *Opt. Express* **2014**, *22*, 4301–4306.

(32) Bachman, K. A.; Peltzer, J. J.; Flammer, P. D.; Furtak, T. E.; Collins, R. T.; Hollingsworth, R. E. Spiral plasmonic nanoantennas as circular polarization transmission filters. *Opt. Express* **2012**, *20*, 1308–1319.

(33) Liao, W.-C.; Liao, S.-W.; Chen, K.-J.; Hsiao, Y.-H.; Chang, S.-W.; Kuo, H.-C.; Shih, M.-H. Optimized Spiral Metal-Gallium-Nitride Nanowire Cavity for Ultra-High Circular Dichroism Ultraviolet Lasing at Room Temperature. *Scientific Reports* **2016**, *6*, 26578.

(34) Yu, C. L.; Liao, S.-W.; Hsiao, Y.-H.; Kuo, H.-C.; Shih, M.-H. Circular Polarized Lasing Characteristics in Metal/GaN Double-Spiral Nanowire Cavity. Conference on Lasers and Electro-Optics. 2017; p STh1C.4.

(35) van der Laan, J. D.; Wright, J. B.; Scrymgeour, D. A.; Kemme, S. A.; Dereniak, E. L. Evolution of circular and linear polarization in scattering environments. *Opt. Express* **2015**, *23*, 31874–31888.

(36) Jin, J.; Luo, J.; Zhang, X.; Gao, H.; Li, X.; Pu, M.; Gao, P.; Zhao, Z.; Luo, X. Generation and detection of orbital angular momentum via metasurface. *Scientific Reports* **2016**, *6*, 24286.

(37) Tanaka, A.; Chen, R.; Jungjohann, K. L.; Dayeh, S. A. Strong Geometrical Effects in Submillimeter Selective Area Growth and Light Extraction of GaN Light Emitting Diodes on Sapphire. *Scientific Reports* **2015**, *5*, 17314.

Graphical TOC Entry